Superconductivity and non-Fermi-liquid behavior of $La_3Pd_4Si_4$ and $Ce_3Pd_4Si_4$

F. Kneidinger, H. Michor, and E. Bauer
Institute of Solid State Physics, Vienna University of Technology, A-1040 Wien, Austria

A. Gribanov, A. Lipatov, and Y. Seropegin
Department of Chemistry, Moscow State University, GSP-1, 119991 Moscow, Russia

J. Sereni
Div. Bajas Temperaturas, CAB-CNEA, 8400 San Carlos de Bariloche, Argentina

P. Rogl
Institute of Physical Chemistry, University of Vienna, A-1090 Wien, Austria
(Received 15 April 2013; published 19 July 2013)

Measurements of temperature and field dependent bulk properties have been carried out on $\{Ce,La\}_3Pd_4Si_4$. Rietveld refinements of x-ray powder intensity data confirm the orthorhombic $U_3Ni_4Si_4$-type structure for both compounds. While $La_3Pd_3Si_4$ exhibits superconductivity below 2 K together with some indications of a two gap scenario, the former can be characterized as a Kondo lattice system in presence of crystalline electric field splitting. Due to the closeness of a quantum critical point, distinct non-Fermi-liquid features dominate the low temperature physics of $Ce_3Pd_4Si_4$.

DOI: 10.1103/PhysRevB.88.024423 PACS number(s): 71.27.+a, 71.20.Lp, 72.15.Qm, 74.70.Dd

I. INTRODUCTION

Intermetallic compounds with a composition of $RE_3T_4X_4$ (RE = rare earth, T = transition metal, X = Si, Ge, Sn) became the subject of intense research, partly because of the variety of magnetic structures[1–5] and partly because of superconductivity occurring in four members of this series with RE = La, T = Ni, Pd, and X = Si, Ge.[6–10] Transport and magnetic properties of the compounds containing magnetic rare earth elements are governed by the RKKY interaction in presence of strong crystalline electric field effects. While the compounds with heavy rare earth elements and X = Ge and Sn crystallize in the $Gd_3Cu_4Ge_4$ type of structure,[1–3] Ge based ternary compounds seem not to exist for the light rare earth based metals.[3] Sn compounds with Pr and Nd, however, do exist.[4]

Ternary La-based systems with T = Pd and Ni and X = Si and Ge have been reported to crystallize in the orthorhombic $U_3Ni_4Si_4$ type of structure and superconductivity was observed for each member of this family, with T_c ranging from $T_c = 2.5$ K ($La_3Pd_4Ge_4$) to $T_c = 0.76$ K ($La_3Ni_4Ge_4$).[9] Fuji *et al.*[6] reported type II superconductivity for $La_3Pd_4Si_4$, with $T_c = 2.15$ K from resistivity and magnetic susceptibility measurements. $Ce_3Ni_4Si_4$ and $Ce_3Rh_4Si_4$ were found to crystallize in the $U_3Ni_4Si_4$ structure, too.[11]

In our previous work on the system Ce-Pd-Si[12] we reported on the existence of $Ce_3Pd_4Si_4$ with $U_3Ni_4Si_4$ type observed from both x-ray powder and single crystal diffraction data, as well as from scanning electron microscopy (SEM). The crystal structure of the compound was solved from single crystal data: space group $Immm$; $a = 0.41618(1)$, $b = 0.42640(1)$, $c = 2.45744(7)$ nm.[12] The structure of $U_3Ni_4Si_4$ can be explained as a combination of AlB_2-type and $BaAl_4$-type layers.[13] The unit cell and crystal structure packing of $Ce_3Pd_4Si_4$ is shown in the inset of Fig. 1. Layers of the ordered derivative from the $BaAl_4$ type, i.e., the $ThCr_2Si_2$ type was used as better choice for illustrating the ternary compound.

In the present paper we report on the results of field and temperature dependent electrical resistivity, magnetic susceptibility, and specific heat measurements of $Ce_3Pd_4Si_4$ at low temperatures in order to derive information about the ground state properties of this ternary compound. Data were analyzed in comparison with isostructural $La_3Pd_4Si_4$, representing the nonmagnetic background of this material, revealing clear signatures of a non-Fermi-liquid state in terms of the spin fluctuation theory by Moriya and Takimoto.[14] In addition, we have studied $La_3Pd_4Si_4$ in some detail to evaluate the superconducting properties of this compound. Interestingly, the heat capacity and the upper critical magnetic field do not follow the predictions of a fully gapped *s*-wave state; rather, a two gap model is better suited to describe the temperature dependent specific heat, in line with a pronounced positive curvature of the upper critical magnetic field.

II. EXPERIMENT

Polycrystalline samples with stoichiometric composition $RE_3Pd_4Si_4$ (RE = La, Ce), each of a weight of 1 g, were prepared by argon arc melting from high-purity elements (99.9 mass% rare-earth elements, 99.999 mass% Si, and 99.99 mass% Pd), on a water-cooled copper hearth. The melting was repeated several times with the button turned over between each melting. The weight loss was less than 0.5 mass%. After melting, the alloys were vacuum sealed in a quartz tube and annealed at 800 °C for 30 days before being quenched in cold water. Both samples were examined by x-ray powder diffraction (XRD). Data were collected at room temperature employing a STOE STADI P diffractometer with a linear PSD and Cu$K_{\alpha 1}$ radiation. Quantitative Rietveld refinement of the x ray was performed with the program FULLPROF,[15,16] employing internal tables for x-ray atomic form factors. Lattice parameters were calculated using program STOE-WINXPOW.[17]

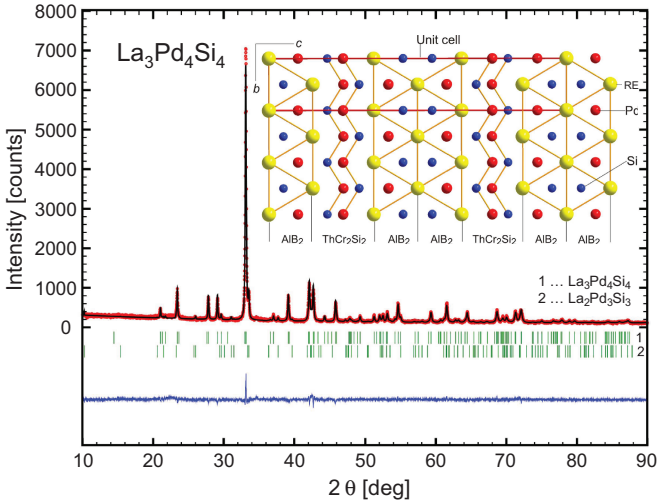

FIG. 1. (Color online) X-ray powder pattern and Rietveld refinement of $La_3Pd_4Si_4$. The inset is a sketch of the crystal structure in projection along [100].

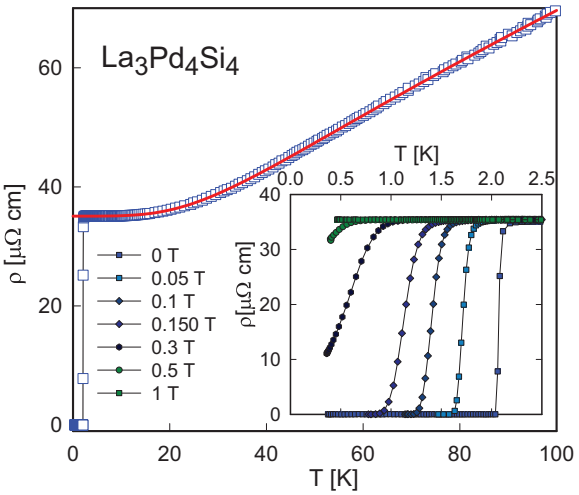

FIG. 2. (Color online) Temperature dependent electrical resistivity ρ of $La_3Pd_4Si_4$. The solid line is a least-squares fit as explained in the text. The inset shows $\rho(T)$ of $La_3Pd_4Si_4$ at various externally applied magnetic fields.

A superconducting quantum interference device (SQUID) magnetometer was used to study magnetic properties from 2.5 up to 300 K in fields up to 6 T using polycrystalline specimens of about 20 mg. Specific heat measurements on about 1 g of polycrystalline $Ce_3Pd_4Si_4$ were performed at temperatures ranging from 2.5 up to 100 K by means of an adiabatic step heating method. Additionally, specific heat measurements in the temperature range between 350 mK and 20 K were carried on $La_3Pd_4Si_4$ and $Ce_3Pd_4Si_4$ samples with a commercial Quantum Design PPMS ^{3}He relaxation calorimeter in fields up to 1 T. Electrical resistivity measurements were carried out in a ^{3}He bath top-loading cryostat with a maximum magnetic field of 12.5 T and for temperatures from 350 mK up to 300 K. Resistivity was measured with the electrical current flowing parallel to the applied magnetic field via a four-probe technique using an ac bridge (Lakeshore 370).

III. RESULTS AND DISCUSSION

The XRD analyses indicate that $RE_3Pd_4Si_4$ phases with La and Ce as rare earth elements are present as a major phase with a minor amount of impurity phases. The XRD pattern of $La_3Pd_4Si_4$ together with the corresponding Rietveld refinement are shown in Fig. 1, revealing $a = 0.42358(1)$ nm, $b = 0.42900(1)$ nm, and $c = 2.45400(7)$ nm. Some small extra XRD peaks could be indexed on the basis of a $La_2Pd_3Si_3$ phase. The content of impurities is estimated to be a few percent in each sample. In the case of $Ce_3Pd_4Si_4$ these small impurity phases were identified as $Ce_2Pd_3Si_3$ ($Ce_2Rh_{1.35}Ge_{4.65}$ type) and $CePd_2Si_2$ ($ThCr_2Si_2$ type) in agreement with the Ce-Pd-Si phase diagram[3], where these two phases were reported as neighboring phases.

A. $La_3Pd_4Si_4$

Both resistivity and heat capacity measurements carried out on $La_3Pd_4Si_4$ evidence bulk superconductivity below 2 K. Shown in Fig. 2 is the temperature dependent electrical resistivity ρ of $La_3Pd_3Si_3$ at zero field (main panel) and at various externally applied magnetic fields. Clearly visible is a superconducting transition being located slightly above 2 K. This transition temperature is in good coincidence with data reported in Refs. 6 and 7 derived from measurements of the electrical resistivity and magnetic susceptibility. Metallic behavior and the importance of s-d scattering in $La_3Pd_3Si_4$ is quantitatively revealed from the applicability of the Bloch-Wilson model,[18] i.e.,

$$\rho(T) = A\left(\frac{T}{\theta_D}\right)^5 \int_0^{\theta_D/T} \frac{z^5 dz}{[\exp(z)-1][1-\exp(-z)]} + B\left(\frac{T}{\theta_D}\right)^3 \int_{\theta_{\min}/T}^{\theta_D/T} \frac{z^3 dz}{[\exp(z)-1][1-\exp(-z)]} - \kappa T^3. \quad (1)$$

The Mott-Jones term κT^3 accounts for scattering of conduction electrons on a narrow d band (e.g., Pd-4d or La-5d in $La_3Pd_3Si_4$) near to the Fermi energy[19] and explains the negative curvature in $\rho(T)$ at higher temperatures. A least-squares fit of this model to the experimental data (solid line, Fig. 2) reveals a Debye temperature $\theta_D = 155$ K, and $\kappa \approx 10^{-7}$ $\mu\Omega$ cm K^{-3} as well as a minimum phonon energy $k_B\theta_{\min} = \hbar\omega_{\min}$, with $\theta_{\min} = 98$ K. Here $\omega_{\min}$ is the frequency corresponding to the minimum $\vec{q}$ value to excite the s-d transitions.[18] $A = 54$ $\mu\Omega$ cm and $B = 8.6$ $\mu\Omega$ cm are material dependent constants (compare Fig. 5, too).

The superconducting phase transition is relatively sharp, evidencing good sample quality. The application of magnetic fields (inset, Fig. 2) consecutively suppresses superconductivity, and magnetic fields of the order of 1 T are sufficient to entirely eliminate the superconducting state. This suppression is accompanied by a slight increase of the width of the phase transition. The Debye temperature as derived from resistivity data is significantly lower than that derived from our specific heat measurements (see below). This might be a result of

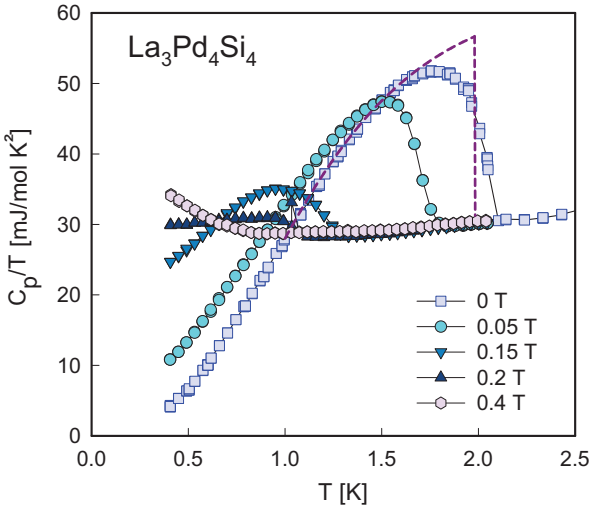

FIG. 3. (Color online) Temperature dependent heat capacity C_p of $La_3Pd_4Si_4$ plotted as C_p/T vs T for various externally applied magnetic fields. The dashed line represents an ideal superconducting transition with $T_c = 1.98$ K.

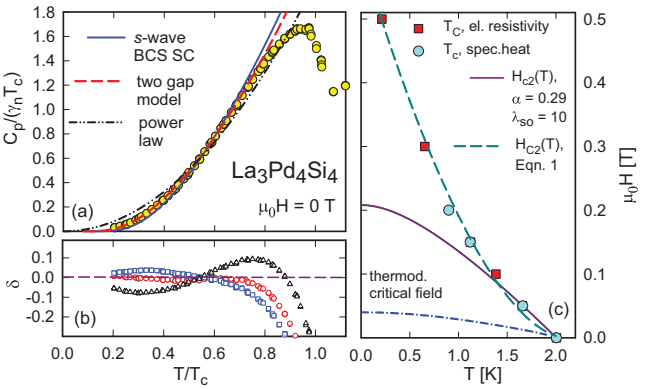

FIG. 4. (Color online) (a) Low temperature specific heat C_p of $La_3Pd_4Si_4$ plotted in a normalized representation $C_p/(\gamma_n T_c)$ vs T/T_c. γ_n is the Sommerfeld constant in the normal state region of $La_3Pd_4Si_4$. The solid line is the heat capacity of a fully gapped BCS superconductor, whereas the dashed line represents a model with two different superconducting gaps. For details see the text. The dashed–double-dotted line is a power law $C_p \propto T^3$. (b) Temperature dependent difference δ of experimental and theoretical heat capacity data $C_p/(\gamma_n T_c)$ below T_c. The colors refer to (a). (c) Upper critical magnetic field $\mu_0 H_{c2}$ of $La_3Pd_4Si_4$ as derived from resistivity (50% criterion) and specific heat data (thermodynamic mean value of the transition). The dashed line is a least-squares fit employing Eq. (1) and the solid line is a fit based on the WHH model (see text). The dashed-dotted line is the thermodynamic critical field.

non-negligible electron-electron scattering superimposed to electron-phonon scattering.

To proof whether superconductivity in $La_3Pd_4Si_4$ is of bulk nature and does not refer to an impurity phase, heat capacity measurements $C_p(T)$ have been carried out for temperatures down to 350 mK and for magnetic fields up to 0.4 T. Results are displayed in Fig. 3. Bulk superconductivity is obvious from the distinct anomaly of C_p/T around 2 K. An accurate determination of the superconducting transition temperature can be made from an idealized jump of the heat capacity anomaly (solid line, Fig. 3) by a balance of entropy, yielding $T_c = 1.98$ K, in good agreement with the resistivity data. The ideal peak height of the SC anomaly would then be 27 mJ/mol K^2.

An estimation of the normal state Sommerfeld value γ_n within the temperature range between 2 and 5 K, reveals 26 mJ/mol K^2, and, additionally, $\theta_D = 280$ K. A similar γ value is obtained if field measurements (e.g., $\mu_0 H = 0.4$ T) are considered, resulting in $\gamma_n = 28$ mJ/mol K^2. The latter, however, is derived within a much smaller range of extrapolation.

From the jump of the specific heat $\Delta C_p/T(T = T_c) \approx 27$ mJ/mol K^2, we calculate the parameter $\Delta C_p/(\gamma_n T_c) \approx 1.03$, which is below the figure expected from BCS theory, $\Delta C_p/(\gamma T_c) \approx 1.43$.

Deviations from a standard BCS behavior are also evident from the temperature dependent specific heat. Compared in Fig. 4(a) are the experimental heat capacity data of $La_3Pd_4Si_4$ plotted in a normalized representation $C_p/(\gamma_n T_c)$, together with the heat capacity of a fully gapped s-wave superconductor as tabulated by Mühlschlegel[20] [solid line, Fig. 4(a)] and a simple power law $C_p \propto T^3$ [dashed–double-dotted line, Fig. 4(a)]. The latter would indicate point nodes in the superconducting gap. Obviously both models do not properly account for the experimental data, specifically in the low temperature range.

A further model calculation is based on a two gap scenario employing the so-called α model developed by Padamsee *et al.*[21] with only one adjustable parameter $\alpha = \Delta(0)/(k_B T_c)$. Note, the value $\alpha = 1.764$ corresponds to the weak coupling BCS limit. The heat capacity in the superconducting state is then a sum of individual contributions of both gaps $\Delta_i(0)$, together with the ratio γ_1/γ_2, with the partial specific heat contributions $\gamma_1 + \gamma_2 = \gamma_n$. Such calculations have been successfully applied to MgB_2,[22] to borocarbide superconductors,[23] or recently to the ternary iron-silicide $Lu_2Fe_3Si_5$.[24] Employing this model to $La_3Pd_4Si_4$ with $\alpha_1 = 1.95$, $\alpha_2 = 1.1$, and $\gamma_1/\gamma_2 = 0.7/0.3$ [dashed line, Fig. 4(a)] reveals convincing agreement with the experimental data in an extended temperature range. Such a two gap model would also be in line with the pronounced positive curvature found for the upper critical field of $La_3Pd_4Si_4$ (see below). The temperature dependent difference between the experimental data and the three theoretical models are shown in Fig. 4(b), clearly demonstrating the superior agreement of the two gap scenario over a fully gapped s-wave model or the simple power law.

As shown in Fig. 3, both the transition temperature and the jump of the specific heat at T_c become suppressed with increasing externally applied magnetic fields. This field dependent lowering of T_c is outlined in Fig. 4(b), where both resistivity and heat capacity data are summarized. As it is obvious from this figure, $T_c(\mu_0 H)$ shows a superlinear dependence, reaching an upper critical field at zero temperature $\mu_0 H_{c2}(0)$ of about 0.6 T. A typical BCS superconductor, however, would exhibit a sublinear temperature dependence $\mu_0 H_{c2}(T)$. In absence of low temperature measurements, Fujii[6,7] estimated an upper

critical field $\mu_0 H_{c2} \approx 0.33$ T from a simple extrapolation of susceptibility results.

The unusual temperature dependence of the upper critical field of $La_3Pd_4Si_4$ can have different microscopic origins: (i) The existence of more than one Fermi-surface sheet with energy gaps of different magnitudes as reported, e.g., for binary MgB_2, or (ii) strong anisotropies of the superconducting order parameter residing on a single Fermi-surface sheet.

Positive curvatures of $\mu_0 H_{c2}(T)$ have been observed, e.g., for the nonmagnetic rare-earth nickel borocarbides RNi_2B_2C (R = Y, Lu) and were explained theoretically employing effective two-band models.[25,26] Phenomenologically, $\mu_0 H_{c2}(T)$ of borocarbides and MgB_2 were accounted for in a wide temperature range using the simple expression[27]

$$\mu_0 H_{c2} = \mu_0 H^*_{c2}(1 - T/T_c)^{1+\beta}, \tag{2}$$

where $\mu_0 H^*_{c2}$ and β are fitting parameters. Similar to the borocarbide case and MgB_2, $\mu_0 H_{c2}(T)$ of $La_3Pd_4Si_4$, as displayed in Fig. 4(c), can be described on the basis of Eq. (2). A least-squares fit is shown in Fig. 4(c) as a dashed line revealing $H^*_{c2} = 0.6$ and $\beta = 0.77$. Exponents of a similar order were derived for borocarbides and MgB_2, too.

Werthamer *et al.*[28] derived an expression (abbreviated as *WHH model*) for the upper critical field $\mu_0 H_{c2}$ in terms of orbital pair breaking, including the effect of Pauli spin paramagnetism and spin-orbit scattering. The WHH model is ruled by two parameters, namely α_M, the Pauli paramagnetic limitation (= Maki parameter[29]), and λ_{so}, describing spin-orbit scattering. While the value of α_M allows a rough discrimination between orbital pair breaking and Pauli limiting, λ_{so} becomes non-negligible for heavier atoms.

The Maki parameter α_M can be estimated[28] from the Sommerfeld value γ and the residual resistivity ρ_0 as $\alpha_M = 0.23$. The reasonably low value of α indicates that orbital pair breaking in $La_3Pd_4Si_4$ is the essential mechanism, limiting the upper critical field. The overall temperature dependence of $\mu_0 H_{c2}$ as derived from the WHH model is displayed as a solid line in Fig. 4(b), revealing $\mu_0 H_{c2}(0) = 0.21$ T, which is more than two times smaller than the experimentally observed data.

The thermodynamic critical field is calculated from the free energy difference between the superconducting and normal state, given by the expression $\Delta F(T) = F_n - F_s = \mu_0 H_c^2(T)/2 = \int_{T_c}^{T} \int_{T_c}^{T'} \frac{(C_s - C_n)}{T''} dT'' dT'$. The quantity $C_s(T)$ is obtained from the zero field specific heat measurement, whereas $C_n(T)$ is obtained from the data corresponding to the 0.4 T run. The values derived are displayed in Fig. 4(b) as a dashed-dotted line; an extrapolation to $T \to 0$ yields $\mu_0 H_c(0) \approx 0.04$ T. This allows us to evaluate a value for the dimensionless Ginzburg Landau parameter $\kappa_{GL} = H_{c2}(0)/(\sqrt{2} H_c) \simeq 9.8$, where the experimentally determined $H_{c2}(0) = 0.55$ T has been used. The coherence length ξ_0 for $T \to 0$ can be obtained from $\mu_0 H_{c2} = \Phi_0/(2\pi\xi_0^2)$, yielding $\xi_0 \simeq 2.44 \times 10^{-8}$ m. Combining the Ginzburg Landau parameter with the coherence length, the London penetration depth can be obtained as $\lambda_L(T \to 0) \simeq 2.39 \times 10^{-7}$ m.

An estimation of the electron-phonon interaction strength $\lambda_{e,ph}$ is possible in terms of the McMillan formula.[30] Applying this model, and taking the repulsive screened Coulomb part $\mu^* \approx 0.13$, yields $\lambda_{e,ph} \approx 0.52$; this characterizes $La_3Pd_4Si_4$ as a SC in the weak coupling limit.

Similarly, an electron-phonon enhancement factor of about the same magnitude can be found if recent electronic structure calculations are considered,[31] where the calculated density of states at the Fermi energy corresponds to a bare band value $\gamma_b = 19.8$ mJ/mol K^2. A comparison with the experimentally derived Sommerfeld value $\gamma = 29$ mJ/mol K^2 yields $\lambda_{e,ph} \approx 0.46$, supporting the weak coupling regime.

Based on the value of $l_{tr}/\xi \approx 0.75$ we classify $La_3Pd_4Si_4$ as a weakly coupled superconductor in the dirty limit; the value of $\kappa_{GL} \approx 10$ refers to a type II superconductor.

B. $Ce_3Pd_4Si_4$

Intermetallic compounds based on Ce are known a long time for a variety of interesting ground states, primarily triggered by the Kondo effect as a result of distinct interactions between conduction electrons and the magnetic moment of the Ce ion. In the following, results derived from resistivity, heat capacity, and magnetization measurements will be used to obtain information on the ground state properties of $Ce_3Pd_4Si_4$.

Shown in Fig. 5 are temperature dependent resistivity measurements of $Ce_3Pd_4Si_4$ and of $La_3Pd_4Si_4$; the latter compound serves as a nonmagnetic reference, representing the contribution to the electrical resistivity owing to the electron-phonon interaction. While $\rho(T)$ of $La_3Pd_4Si_4$ exhibits superconductivity below 2 K and a simple metallic behavior in the normal state region (see the previous section), $\rho(T)$ of $Ce_3Pd_4Si_4$ shows a much more complex temperature dependence as typical for Kondo lattice systems. The most dominant feature is a maximum in $\rho(T)$ around 8.5 K with $\rho(T)$ dropping above and below this temperature. Well above 100 K, a local minimum develops in $\rho(T)$. A comparison of the experimental data of $Ce_3Pd_4Si_4$ and $La_3Pd_4Si_4$ allows

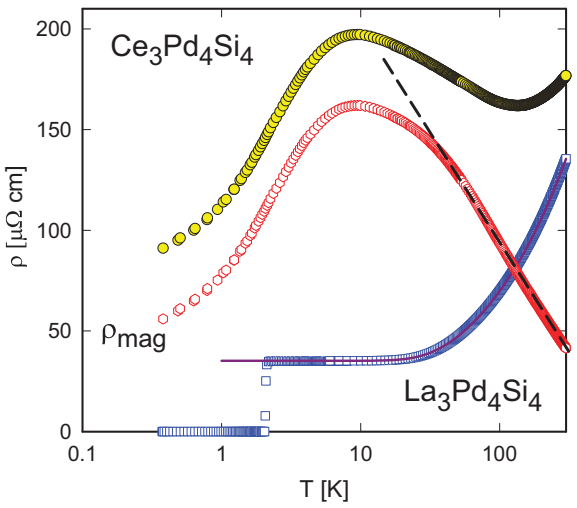

FIG. 5. (Color online) Temperature dependent resistivity ρ of $La_3Pd_4Si_4$ and $Ce_3Pd_4Si_4$ plotted on a logarithmic temperature scale. The magnetic contribution $\rho_{mag}(T)$ of $Ce_3Pd_4Si_4$ is also shown in this plot, where the dashed line should emphasize Kondo interaction; $\rho_{mag} \approx \rho(Ce_3Pd_4Si_4) - \rho(La_3Pd_4Si_4)$. The solid line is a least-squares fit as explained in Fig. 2.

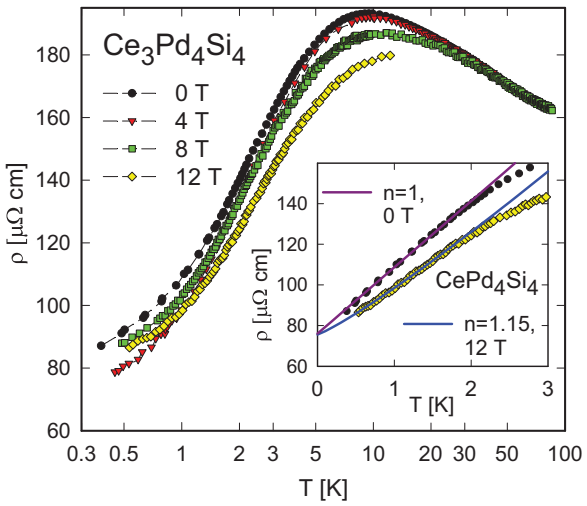

FIG. 6. (Color online) Low temperature electrical resistivity ρ measured at various externally applied magnetic fields. The inset shows resistivity details together with power law fits for the zero and 12 T run.

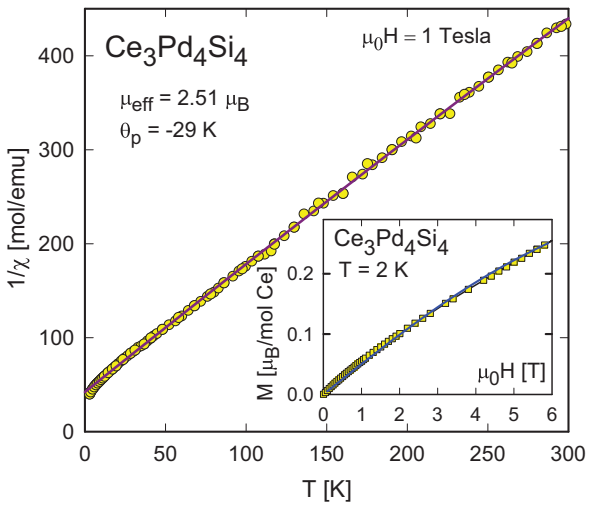

FIG. 7. (Color online) Temperature dependent magnetic susceptibility χ of $Ce_3Pd_4Si_4$ plotted as $1/\chi$ vs T. The solid line is a fit employing a modified Curie-Weiss law. The inset displays the isothermal magnetization ($T = 2$ K) of $Ce_3Pd_4Si_4$; the solid line is the magnetization of an effective spin 1/2 system with a Landè factor $g_{\text{eff}} = 0.775$.

us to derive the magnetic part ρ_{mag} if one assumes that the phonon contribution of both compounds is equal. $\rho_{\text{mag}}(T)$ of $Ce_3Pd_4Si_4$ is included in Fig. 5, too. The logarithmic temperature dependence of ρ_{mag} at elevated temperatures evidences Kondo interaction in the presence of crystalline electric field splitting. The drop of $\rho(T)$ at low temperatures results from the development of a coherent state owing to the Kondo lattice properties of $Ce_3Pd_4Si_4$. In general, such a coherent state would be concomitant with Fermi-liquid features, and a T^2 behavior of $\rho_{\text{mag}}(T)$ should become obvious. The present experimental data, however, reveal a distinctly different power law.

A closer inspection of the low temperature resistivity data is shown in Fig. 6, where measurements at various magnetic fields are added. The low temperature maximum in $\rho(T)$ is weakly field dependent and shifts from about 8.5 K at zero magnetic field to about 10.5 K at an externally applied field of 8 T. Such a field dependence of the electrical resistivity is typical for cerium and ytterbium based Kondo lattices. At the lowest temperatures of our study, Fermi-liquid features are absent in $\rho(T)$. Rather, the zero field measurement can be accounted for by a simple power law $\rho(T) = \rho_0 + AT^n$, where the exponent $n = 1$ reveals best agreement; in the case of the 12 T run, $n = 1.15$. These exponents are indicative of a non-Fermi-liquid behavior, arising, most likely, from the proximity of a magnetic instability of the Ce ions.

A magnetic state of the Ce ions in $Ce_3Pd_4Si_4$, can be concluded from magnetic susceptibility measurements $\chi(T)$ as shown in Fig. 7. Applying a modified Curie-Weiss law to the experimental data, i.e.,

$$\chi = \chi_0 + \frac{C}{T - \theta_p}, \tag{3}$$

yields information concerning a temperature independent Pauli contribution χ_0, the effective magnetic moment μ_{eff} (deduced from the Curie constant C), and the paramagnetic Curie temperature θ_p. Results of a least-squares fit ($T > 50$ K) according to Eq. (3) are shown as a solid line in Fig. 7, revealing an effective magnetic moment $\mu_{\text{eff}} = 2.51\ \mu_B$ close to that of the Ce-$4f^1$ electronic configuration [$\mu_{\text{eff}}(Ce^{3+}) = 2.54\ \mu_B$] and a paramagnetic Curie temperature $\theta_p = -29$ K. The latter refers to antiferromagnetic interactions among the Ce ions. $\chi(T)$ at low temperatures does not show any characteristic anomaly being typical for long range magnetic order. This is in line with isothermal magnetization data taken at $T = 2$ K (inset, Fig. 7). A smooth, slightly curvilinear $M(H)$ dependence is observed with relatively small magnetization values at 6 T. A description of these data can be done calculating the field dependent magnetization of an effective spin 1/2 system at $T = 2$ K, employing a Landè factor $g_{\text{eff}} = 0.775$. Fairly good agreement is obtained in this way, except for the low field range, where the disagreement between the model and the experimental data appears to be in line with the Curie-like bending of the magnetic susceptibility at low temperatures. CEF effects are the primary cause for the appearance of only small magnetization values, well below $g_j j = 2.14\ \mu_B$, associated with the total angular momentum of the free Ce^{3+} ion. A comparison with magnetization data of $Ce_3Pd_4Ge_4$ at $T = 2$ K[35] shows for the latter a clear indication for a metamagnetic phase transition around 4 T, thus referring to an antiferromagnetic ground state.

To further prove the ground state of $Ce_3Pd_4Si_4$, heat capacity measurements C_p have been performed down to 400 mK. Results are displayed in Fig. 8 as C_p/T vs T, together with those of $La_3Pd_4Si_4$. The most prominent feature is an almost logarithmic contribution in the range of a few Kelvin, followed by a smooth saturation of C_p/T towards zero with very large values of about 2.7 J/mol K^2, corresponding to $\gamma = 0.9$ J/mol K^2 per cerium ion. Considering renormalization group calculations by Oliveira and Wilkins,[32] the Kondo temperature T_K follows from $T_K = 0.68 \cdot R/\gamma = 6.2$ K if a doublet is considered as ground state.

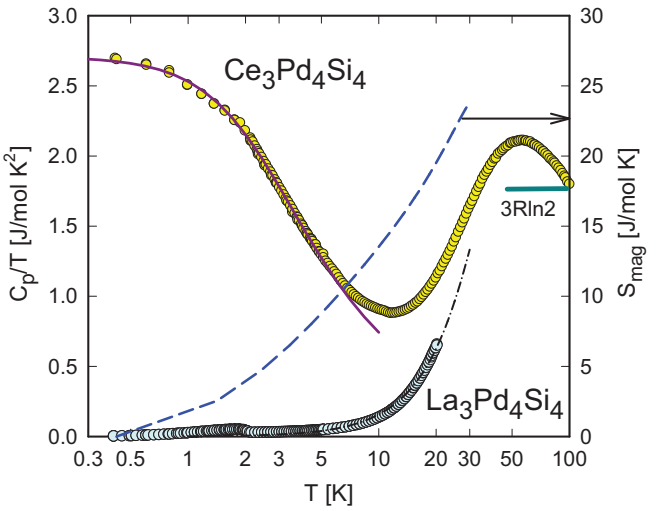

FIG. 8. (Color online) Temperature dependent specific heat C_p of $Ce_3Pd_4Si_4$ plotted as C_p/T vs $\ln T$. For purpose of comparison, C_p/T of $La_3Pd_4Si_4$ is added, too. The solid line represents the heat capacity of a spin fluctuation model according to Eq. (2) near to the quantum critical point and the dashed-dotted line is a smooth extrapolation of heat capacity data using the Debye model with $\theta_D = 280$ K. The dashed line is the calculated magnetic entropy $S_{\rm mag}$ of $Ce_3Pd_4Si_4$, referring to the right axis.

Assuming that the phonon contribution to the heat capacity of $Ce_3Pd_4Si_4$ can be represented by the specific heat of $La_3Pd_4Si_4$, the magnetic entropy $S_{\rm mag}$ can be derived by integrating $C_{\rm mag}/T$. Results of this evaluation are plotted in Fig. 8 as a dashed line, referring to the right axis. An entropy of $3 \cdot R \ln 2$ is reached around 18 K. The slow rate of the recovery of magnetic entropy in $Ce_3Pd_4Si_4$ is a consequence of the Kondo effect present in this compound. $S_{\rm mag}(T)$ also allows us to estimate the Kondo temperature independently from $T_K = T(S_{\rm mag} \approx 0.45 \cdot R \ln 2) \approx 4.4$ K,[33] in very good agreement with the estimation obtained from the Sommerfeld value. Kondo-type interaction is also supposed to be responsible for the suppression of long range magnetic order, absent in $Ce_3Pd_4Si_4$ at least down to 400 mK.

The further increase of $S_{\rm mag}$ at higher temperatures indicates that the excited crystalline electric field levels are not well separated from the ground state; hence some hybridization between CEF levels might appear. This is seen from some deformation of the maximum of the magnetic contribution to the electrical resistivity, too.

In order to test whether or not $Ce_3Pd_4Si_4$ is at or near the quantum critical point, the self-consistent renormalization (SCR) model of Moriya and Takimoto[14] can be taken into account:

$$C_m = 9N_0 \int_0^{x_0} dx x^2 \left\{ \left[u^2 - 2u\frac{dy}{dt} + \left(\frac{dy}{dt}\right)^2 \right] \times \left[-\frac{1}{u} - \frac{1}{2u^2} + \psi'(u) \right] - t\frac{d^2y}{dt^2} \left[\ln u - \frac{1}{2u} - \psi(u) \right] \right\}, \quad (4)$$

where $x^2 = u \cdot t - y$, $u = u(y)$, and $y = y(y_1, y_0)$ is the reduced staggered susceptibility and $t = T/T_0$. T_0 is some characteristic temperature, scaling a temperature dependent physical quantity; y_1 is a constant. The parameter y_0 measures the distance of the system to the magnetic instability and provides a measure of the inverse correlation length.[34] As y_0 approaches zero, the system approaches the quantum critical point.

An adjustment of Eq. (4) to the experimental data is displayed in Fig. 8 as a solid line, revealing excellent agreement between the data and the model for $T_0 = 3.5$ K, $y_0 = 1.5$, and $y_1 = 15$. The model reveals a constant for $T \to 0$ followed by a $T^{-1/2}$ dependence; finally, at higher temperatures, a logarithmic decrease of C_p/T occurs, in accord with the experimental findings. The finite—although small—value of y_0 indicates that $Ce_3Pd_4Si_4$ is not directly at the QCP; nevertheless it proves that this sample is next to a phase transition at $T = 0$.

A more stable magnetic state, however, was observed for $Ce_3Pd_4Ge_4$,[35] where due to the increase of the unit cell volume owing to the Si/Ge substitution, a decrement of hybridization takes place; as a consequence, magnetic order occurs and the system has moved away from quantum criticality.

IV. SUMMARY

Bulk properties of $REPd_4Si_4$ with RE = La and Ce both with the $U_3Ni_4Si_4$-type structure were investigated by means of resistivity, specific heat, and magnetic susceptibility measurements. Nonmagnetic $La_3Pd_4Si_4$ is characterized by superconductivity below about 2 K. Disagreement from a simple, fully gapped s-wave BCS superconductor are obvious from deviations of the temperature dependent specific heat and from the positive curvature of the upper critical field $\mu_0 H_{c2}$. A two band and two gap model reasonably well describes the heat capacity data in the superconducting state if $\alpha_1 = 1.95$ and $\alpha_2 = 1.1$.

The isostructural Ce-based compound behaves as a Kondo lattice, exhibiting a pronounced maximum in the temperature dependent electrical resistivity as well as an extended logarithmic temperature range as a result of the Kondo effect in presence of crystalline electric field effects. At low temperatures, distinct deviations from a Fermi-liquid ground state are evident in both resistivity and heat capacity data, provoked from the proximity of a phase transition at $T = 0$.

ACKNOWLEDGMENTS

This research was supported by the Austrian FWF project P22295 and by the Austrian-Russian bilateral exchange program OEAD-project I.17/2006. A.G. and Y.S. are thankful to the Russian Foundation for Basic Research (RFBR) for financial support (Grant No. 11-03-01191-a). X-ray investigations were performed at the User Facilities Center of the M. V. Lomonosov Moscow State University under support of the Ministry of Education and Science of Russia, Contract N16.552.11.7081. J.S. and P.R. wish to thank the OEAD, project AR 22/2011.

[1]E. Wawrzynska, S. Baran, J. Leciejewicz, W. Sikora, N. Stüsser, and A. Szytula, J. Phys.: Condens. Mat. **15**, 803 (2003).
[2]E. Wawrzynska, J. Hernandez-Velasco, B. Penc, W. Sikora, A. Szytula, and A. Zygmunt, J. Phys.: Condens. Mat. **15**, 5279 (2003).
[3]G. Bocelli, O. Sologub, and P. Salamakha, J. Alloys Compounds **360**, L3 (2003).
[4]E. Wawrzynska, J. Hernandez-Velasco, B. Penc, and A. Szytula, J. Phys.: Condens. Mat. **16**, 45 (2004).
[5]E. Wawrzynska, J. Hernandez-Velasco, B. Penc, M. Rams, and A. Szytula, J. Magn. Magn. Mater. **288**, 111 (2005).
[6]H. Fujii, T. Mochiku, H. Takeya, and A. Sato, Phys. Rev. B **72**, 214520 (2005).
[7]H. Fujii, J. Phys.: Condens. Matter **18**, 8037 (2006).
[8]T. Mochiku, H. Fujii, H. Takeya, T. Wuernisha, K. Mori, T. Ishigaki, T. Kamiyama, and K. Hirata, Physica C **463–465**, 182 (2007).
[9]S. Kasahara, H. Fujii, H. Takeya, T. Mochiku, A. D. Thakur, and K. Hirata, J. Phys.: Condens. Matter **20**, 385204 (2008).
[10]S. Kasahara, H. Fujii, T. Mochiku, H. Takeya, and K. Hirata, Physica B **403**, 1119 (2008).
[11]P. Rogl, B. Chevalier, and J. Etourneau, J. Solid State Chem. **88**, 429 (1990).
[12]A. Lipatov, A. Gribanov, A. Grytsiv, P. Rogl, E. Murashova, Y. Seropegin, G. Giester, and K. Kalmykov, J. Solid State Chem. **182**, 2497 (2009).
[13]E. Parthe, L. Gelato, B. Chabot, M. Penzo, K. Cenzual, and R. Gladyshevskii, *TYPIX—Standardized Data and Crystal Chemical Characterization of Inorganic Structure Types* (Springer, Berlin, 1994).
[14]T. Moriya and T. Takimoto, J. Phys. Soc. Jpn. **64**, 960 (1995).
[15]T. Roisnel and J. Rodriguez-Carvajal, Mater. Sci. Forum **118**, 378 (2001).
[16]J. Rodríguez-Carvajal, Physica B **192**, 55 (1993).
[17]STOE-WINXPOW (Version 1.06), Stoe & Cie GmbH, Darmstadt, Germany, 1999
[18]A. H. Wilson, Proc. R. Soc. London Ser. A **167**, 580 (1938).
[19]J. C. H. Chiu, Phys. Rev. B **13**, 1507 (1976).
[20]B. Mühlschlegel, Z. Phys., **155**, 313 (1959).
[21]H. Padamsee, J. E. Neighbor, and C. A. Shiffman, J. Low Temp. Phys. **12**, 387 (1973).
[22]F. Bouquet, R. A. Fisher, N. E. Phillips, D. G. Hinks, and J. D. Jorgensen, Phys. Rev. Lett. **87**, 047001 (2001).
[23]C. L. Huang, J.-Y. Lin, C. P. Sun, T. K. Lee, J. D. Kim, E. M. Choi, S. I. Lee, and H. D. Yang, Phys. Rev. B **73**, 012502 (2006).
[24]Y. Nakajima, T. Nakagawa, T. Tamegai, and H. Harima, Phys. Rev. Lett. **100**, 157001 (2008).
[25]S. V. Shulga, S. L. Drechsler, G. Fuchs, K. H. Muller, K. Winzer, M. Heinecke, and K. Krug, Phys. Rev. Lett. **80**, 1730 (1998).
[26]S. Manalo, H. Michor, M. El-Hagary, G. Hilscher, and E. Schachinger, Phys. Rev. B **63**, 104508 (2001).
[27]K.-H. Müller, G. Fuchs, A. Handstein, K. Nenkov, V. N. Narozhnyi, D. Eckert, and M. Wolf, Physica C **372–376**, 1251 (2002); J. Freudenberger, S.-L. Drechsler, G. Fuchs, A. Kreyssig, K. Nenkov, S. V. Shulga, K.-H. Müller, and L. Schultz, *ibid.* **306**, 1 (1998).
[28]N. R. Werthamer, E. Hefland, and P. C. Hohenberg, Phys. Rev. **147**, 295 (1966).
[29]K. Maki, Phys. Rev. **148**, 362 (1966).
[30]W. L. McMillan, Phys. Rev. **167**, 331 (1968).
[31]M. J. Winiarski and M. Samsel-Czekala, J. Alloys Compounds **546**, 124 (2013).
[32]L. N. Oliveira and J. W. Wilkins, Phys. Rev. Lett. **47**, 1553 (1981).
[33]H.-U. Desgranges and K. D. Schotte, Phys. Lett. A **90**, 240 (1982).
[34]E. D. Bauer, V. A. Sidorov, S. Bobev, D. J. Mixson, J. D. Thompson, J. L. Sarrao, and M. F. Hundley, Phys. Rev. B **71**, 014419 (2005).
[35]H. J. Im, Y. S. Kwon, and M. H. Jung, Solid State Commun. **124**, 181 (2002).